THE FINITE-DIFFERENCE TIME-DOMAIN (FD-TD) METHOD FOR NUMERICAL MODELING OF ELECTROMAGNETIC SCATTERING

Allen Taflove, Senior Member, IEEE
Department of Electrical Engineering
and Computer Science
The Technological Institute
Northwestern University
Evanston, IL 60201

Korada R. Umashankar, Senior Member, IEEE
Department of Electrical Engineering
and Computer Science
University of Illinois at Chicago
P. O. Box 4348
Chicago, IL 60680

Abstract

This paper reviews recent applications of the finite-difference time-domain (FD-TD) numerical modeling approach for Maxwell's equations. FD-TD is very simple in concept and execution. However, it is remarkably robust, providing highly accurate modeling predictions for a wide variety of electromagnetic wave interaction problems. The objects modeled to date range from simple 2-D geometric shapes to extremely complex 3-D aerospace and biological systems. Rigorous analytical or experimental validations are provided for the canonical shapes, and it is shown that FD-TD predictive data for near fields and radar cross section (RCS) are in excellent agreement with the benchmark data. It is concluded that, with continuing advances in FD-TD modeling theory for target features relevant to the RCS problem, and with continuing advances in vector- and concurrent-processing supercomputer technology, it is likely that FD-TD numerical modeling will occupy an important place in RCS technology in the 1990's and beyond.

1. Introduction

Accurate numerical modeling of the radar cross section (RCS) of complex electrically-large objects is difficult. Typical structures have shapes, apertures, cavities, and material compositions or coatings which produce near fields that cannot be resolved into finite sets of modes or rays. Proper numerical modeling of such near fields requires sampling at sub-wavelength resolution to avoid aliasing of magnitude and phase information. The goal is to provide a self-consistent model of the mutual coupling of all of the electrically small regions (cells) comprising the structure, even if the structure spans tens of wavelengths in three dimensions.

A candidate numerical modeling approach for this purpose is the finite-difference time-domain (FD-TD) solution of Maxwell's curl equations. This approach is analogous to existing finite-difference solutions of fluid-flow problems encountered in computational aerodynamics in that the numerical model is based upon a direct solution of the governing partial differential equation. Yet, FD-TD is a non-traditional approach to numerical electromagnetic modeling, where frequency-domain approaches have dominated.

One of the goals of this paper is to demonstrate that recent advances in FD-TD modeling concepts and software implementation, combined with advances in computer technology, have expanded the scope, accuracy, and speed of FD-TD modeling to the point where it may be the preferred choice for certain types of scattering problems. With this in mind, this paper will succinctly review the following FD-TD numerical modeling applications dealing with electromagnetic scattering by canonical two- and three-dimensional targets:

a. Circular dielectric / permeable cylinder, conformally modeled

b. Metal cube, broadside incidence

c. Three-dimensional T-shaped conducting target, monostatic RCS pattern

d. Trihedral metal corner reflector, monostatic RCS pattern
   -- Bare metal case
   -- Coated with a commercially available three-layer radar absorbing material (RAM)

Each of these examples compares the FD-TD modeling results with other data obtained via analysis, alternative numerical procedures, or actual measurements. Numerous other examples, including models of non-canonical aerospace and biological structures of great complexity, are available in the references.

2. General Characteristics of FD-TD

As stated, FD-TD is a direct solution of Maxwell's time-dependent curl equations. It employs no potentials. Instead, it applies simple, second-order accurate central-difference approximations [1] for the space and time derivatives of the electric and magnetic fields directly to the respective differential operators of the curl equations. This achieves a sampled-data reduction of the continuous electromagnetic field in a volume of space, over a period of time. Space and time discretizations are selected to bound errors in the sampling process, and to insure numerical stability of the algorithm [2]. Electric and magnetic field components are interleaved in space to permit a natural satisfaction of tangential field continuity conditions at media interfaces. Overall, FD-TD is a marching-in-time procedure which simulates the continuous actual waves by sampled-data numerical analogs propagating in a data space stored in a computer. At each time step, the system of equations to update the field components is fully explicit, so that there is no need to set up or solve a system of linear equations, and the required computer storage and running time is proportional to the electrical size of the volume modeled.

Fig. 1a illustrates the time-domain wave tracking concept of the FD-TD method. A region of space within the dashed lines is selected for field sampling in space and time. At time = 0, it is assumed that all fields within the numerical sampling region are identically zero. An incident plane wave is assumed to enter the sampling region at this point. Propagation of the incident wave is modeled by the commencement of time-stepping, which is simply the implementation of the finite-difference analog of the curl equations. Time-stepping continues as the numerical analog of the incident wave strikes the modeled target embedded within the sampling region. All outgoing scattered wave analogs ideally propagate through the lattice truncation planes with negligible reflection to exit the sampling region. Phenomena such as induction of surface currents, scattering and multiple scattering, penetration through apertures, and cavity excitation are modeled time-step by time-step by the action of the curl equations analog. Self-consistency of these modeled phenomena is generally assured if their spatial

0018-9464/89/0700-3086$01.00

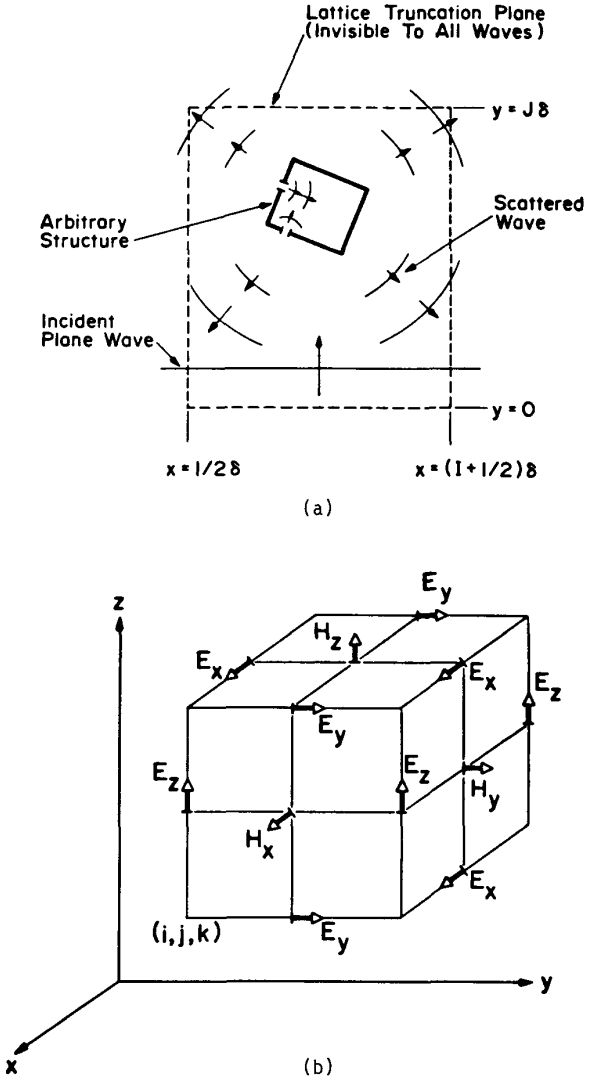

Fig. 1. Basic elements of the FD-TD space lattice: (a) time-domain wave tracking concept; (b) lattice unit cell in Cartesian coordinates [1].

and temporal variations are well resolved by the space and time sampling process.

Time-stepping is continued until the desired late-time pulse response or steady-state behavior is achieved. An important example of the latter is the sinusoidal steady state, wherein the incident wave is assumed to have a sinusoidal dependence, and time-stepping is continued until all fields in the sampling region exhibit sinusoidal repetition. This is a consequence of the limiting amplitude principle [3]. Extensive numerical experimentation with FD-TD has shown that the number of complete cycles of the incident wave required to be time-stepped to achieve the sinusoidal steady state is approximately equal to the Q factor of the structure or phenomenon being modeled.

Fig. 1b illustrates the positions of the electric and magnetic field components about a cubic lattice unit cell [1]. Note that each magnetic field vector component is surrounded by four circulating electric field vector components, and vice versa. This arrangement permits not only a centered-difference analog to the space derivatives of the curl equations, but also a natural geometry for implementing the integral form of Faraday's Law and Ampere's Law at the space cell level. This integral representation permits a simple but effective modeling of the physics of smoothly curved target surfaces, as will be seen later.

Fig. 2 illustrates how an arbitrary three-dimensional scatterer is embedded in an FD-TD space lattice comprised of the unit cells of Fig. 1b. Simply, the desired values of electrical permittivity and conductivity are assigned to each electric field component of the lattice. Correspondingly, desired values of magnetic permeability and equivalent loss are assigned to each magnetic field component of the lattice. The media parameters are interpreted by the FD-TD program as local coefficients for the time-stepping algorithm. Specification of media properties in this component-by-component manner results in a stepped-edge approximation of curved surfaces. Continuity of tangential fields is assured at the interface of dissimilar media with this procedure. There is no need for special field matching at media interfaces. Stepped-edge approximation of curved surfaces has been found to be adequate in the FD-TD modeling problems studied in the 1970's and early 1980's, including wave interactions with biological tissues [4], penetration into cavities [5 - 7], and electromagnetic pulse interactions with complex structures [8 - 10]. However, recent interest in wide dynamic range models of scattering by curved targets has prompted the development of surface-conforming FD-TD approaches which eliminate staircasing. One such will be summarized later in this paper.

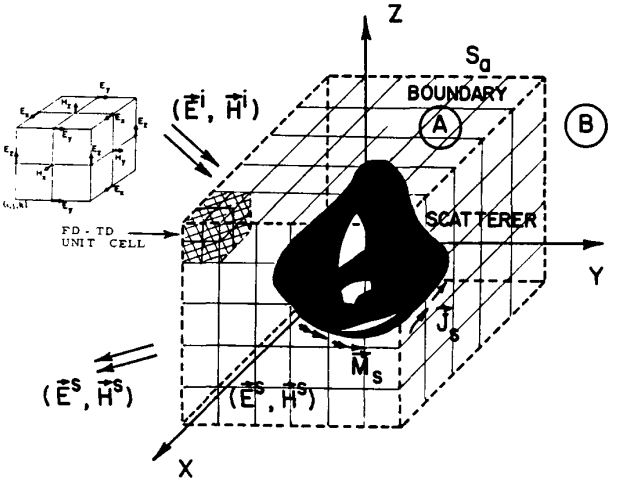

Fig. 2. Arbitrary 3-D scatterer embedded in the FD-TD space lattice.

Fig. 3a illustrates the division of the FD-TD lattice into total-field and scattered-field regions. This division has been found to be very useful since it permits the efficient simulation of an incident plane wave in the total-field region with arbitrary angle of incidence, polarization, time-domain waveform, and duration [11, 12]. Three additional important benefits arise from this lattice division, as follows:

a. A large near-field computational dynamic range is achieved since the scatterer of interest is embedded in the total-field region. Thus, low actual field levels

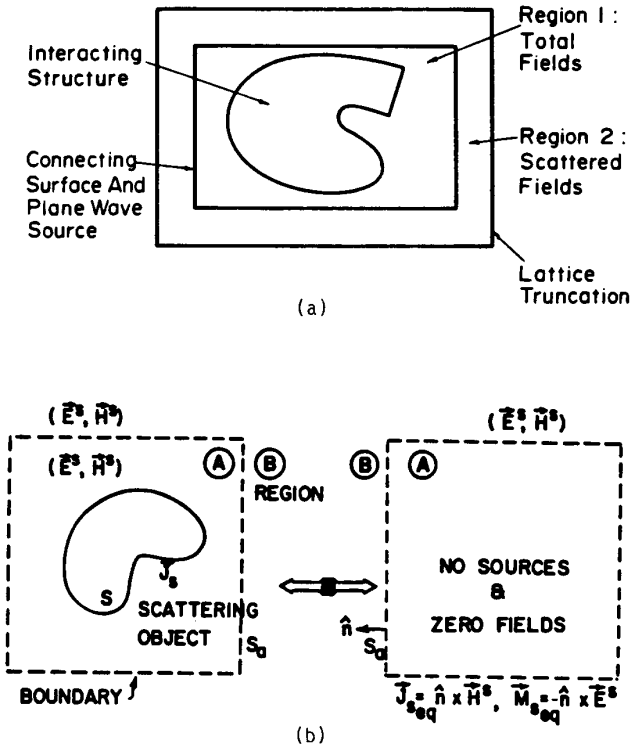

Fig. 3. Zoning of the FD-TD space lattice: (a) total-field and scattered-field regions [11, 12]; (b) near-to-far field integration surface located in the scattered-field region [12].

in shadow regions or within shielding enclosures are computed directly without suffering subtraction noise (as would be the case if scattered fields in such regions were time-stepped via FD-TD, and then added to a cancelling incident field to obtain the low total-field levels.)

b. Embedding the scatterer in the total-field region permits a natural satisfaction of tangential field continuity across media interfaces, as discussed earlier, without having to compute the incident field at possibly numerous points along a complex locus that is unique to each scatterer. The zoning arrangement of Fig. 3a requires computation of the incident field only along the rectangular connecting surface between the total-field and scattered-field regions. This surface is fixed, i.e., independent of the shape or composition of the enclosed scatterer being modeled.

c. The provision of a well-defined scattered-field region in the FD-TD lattice permits the near-to-far field transformation depicted in Fig. 3b. The dashed virtual surface shown here can be located along convenient lattice planes in the scattered-field region of Fig. 3a. Tangential scattered E and H fields computed via FD-TD at this virtual surface can then be weighted by the free-space Green's function and then integrated (summed) to provide the far-field response and RCS (full bistatic response for the assumed illumination angle) [12 - 14]. The near-field integration surface has a fixed rectangular shape, and thus is independent of the shape or composition of the enclosed scatterer being modeled.

Fig. 3a uses the term "lattice truncation" to designate the outermost lattice planes in the scattered-field region. The fields at these planes cannot be computed using the centered-differencing approach because of the assumed absence of known field data at points outside of the lattice truncation. These data are needed to form the central differences. Therefore, an auxiliary lattice truncation condition is necessary. This condition must be consistent with Maxwell's equations in that an outgoing scattered-wave numerical analog striking the truncation must exit the lattice without appreciable non-physical reflection, just as if the lattice truncation was invisible.

It has been shown that the required lattice truncation condition is really a radiation condition in the near field [15 - 17]. A very successful second-order accurate finite-difference approximation of the exact radiation condition in Cartesian coordinates was introduced in [11]. This approximation was subsequently used in a variety of 2-D and 3-D FD-TD scattering codes [12 - 14], yielding excellent results for both near and far fields. (For example, all FD-TD results in this paper were obtained using this approximate radiation condition.) However, recent interest in wide dynamic range models of scattering has prompted research in the construction of even more accurate near-field radiation conditions, including fixed third-order accurate approximations [18, 19], adaptive conditions [20], and predictor-corrector conditions [21]. The goal here is to reduce the numerical lattice background noise due to non-physical reflections of wave analogs at the lattice truncations by at least 20 dB relative to that of [11].

3. Scattering Prediction for Canonical Targets

Analytical, code-to-code, and experimental validations have been obtained relative to FD-TD modeling of a wide variety of 2-D and 3-D structures [22]. Both convex and reentrant (cavity-type) shapes have been studied; and structure material compositions have included perfect conductors, homogeneous and inhomogeneous lossy dielectrics, and anisotropic dielectric and permeable media. Selected past and new validations will be reviewed here.

a. Circular Dielectric / Permeable Cylinder, Conformally Modeled

The interleaving of E and H field components in the FD-TD lattice permits the construction of generalized Faraday's Law and Ampere's Law contour paths which can be adjusted to exactly conform with a smoothly curved target surface. An example of this is shown in Fig. 4. In this manner, slightly modified time-stepping expressions for the field components at or adjacent to the target surface are derived from the integral form of Maxwell's equations. All other field components in the

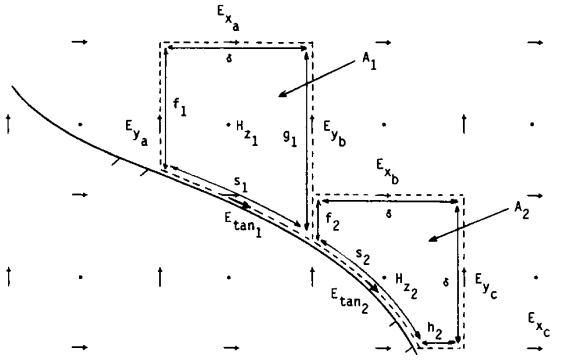

Fig. 4. Faraday's Law contour paths for conformal FD-TD modeling of a smoothly curved target, TE case

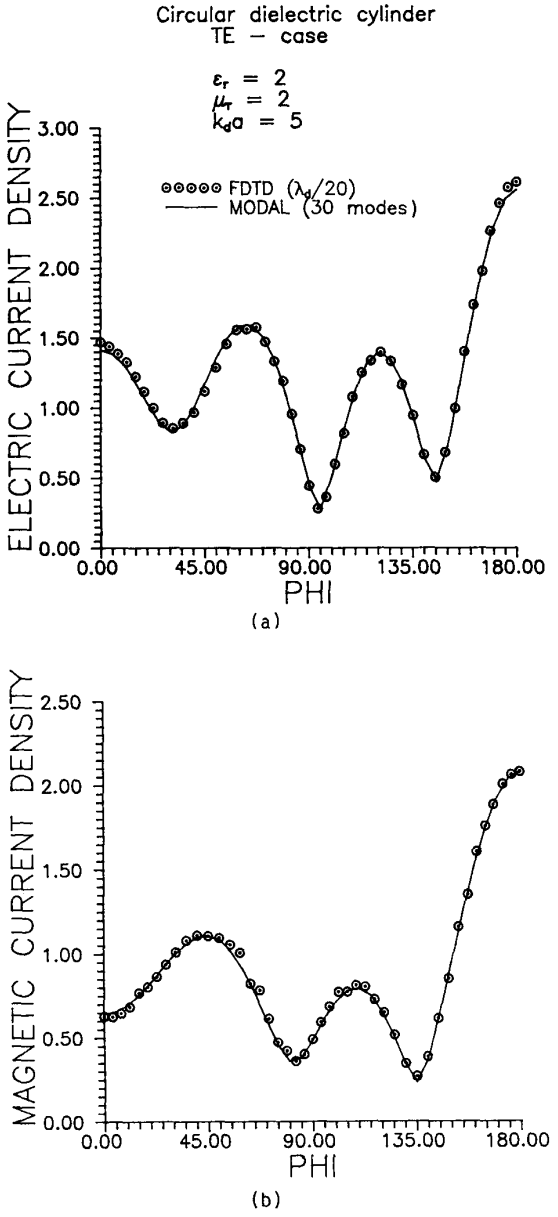

Fig. 5. Comparison of conformal FD-TD model and exact solution for TE illumination of a circular dielectric/permeable cylinder: (a) surface electric currents; (b) surface magnetic currents.

FD-TD lattice are time-stepped in the normal manner. In effect, only the space cells immediately adjacent to the target surface are deformed to conform with the surface.

The accuracy of the conformal FD-TD model is illustrated in Fig. 5. Here, a moderate-resolution Cartesian FD-TD grid (having 1/20 dielectric-wavelength cell size) is used to compute the surface electric and magnetic current distributions induced on a $k_d a = 5$ circular dielectric/permeable cylinder by a TE-polarized incident plane wave. Excellent agreement with the exact modal solution is seen. Note also that the computer running time for the conformal FD-TD model is essentially the same as for the old staircase FD-TD model since only a few field components immediately adjacent to the target surface require a slightly modified time-stepping relation.

b. Metal Cube, Broadside Incidence [13]

Results are now shown for the FD-TD computed surface electric current distribution on a metal cube subject to plane-wave illumination at broadside incidence. The current distribution is compared to that computed by a standard frequency-domain, electric field integral equation (EFIE), triangular surface-patching, method of moments (MoM) code. It is shown that a very high degree of correspondence exists between the two sets of predictive data.

The detailed surface current study involves a metal cube of electrical size $k_0 s = 2$, where s is the side width of the cube. For the FD-TD model, each cube face is spanned by 400 square cells (20 x 20), and the radiation boundary is located at a uniform distance of 15 cells from the cube surface. For the MoM model, each cube face is spanned by either 18 or 32 triangular patches (to test its convergence). Fig. 6 graphs comparative results for the "looping" surface current along the E-plane locus ab'c'd. The FD-TD values agree with the high-resolution MoM data to better than ±2.5% (±0.2 dB) in magnitude and ±1° in phase at all comparison points.

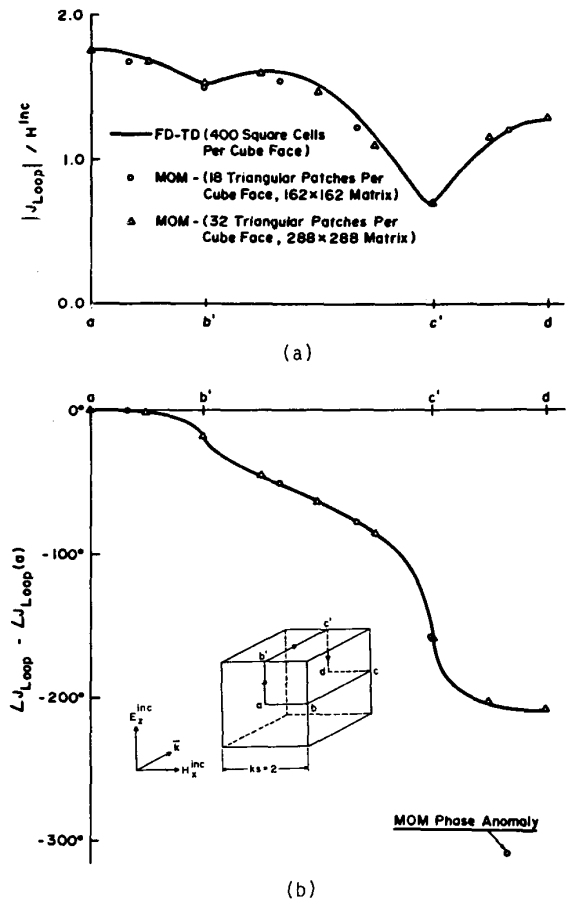

Fig. 6. Comparison of FD-TD and EFIE/MOM results for the "looping" surface electric current along the E-plane locus of a perfectly-conducting cube: (a) magnitude; (b) phase [13].

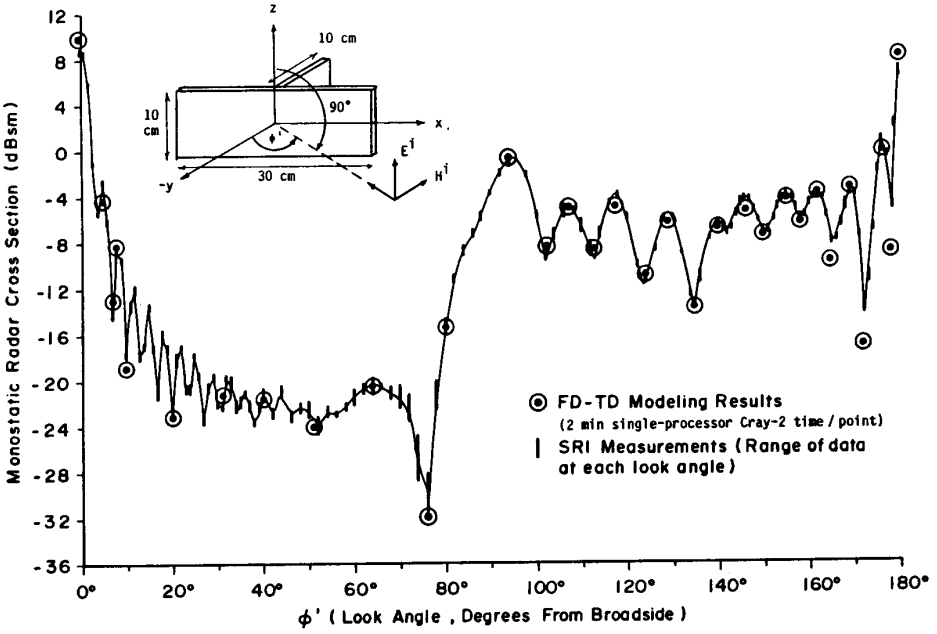

Fig. 7. Experimental validation of FD-TD modeling predictions of monostatic RCS vs. azimuth for the crossed-plate target at 9 GHz (main plate size = 3 x 9 λ_0, bisecting fin size = 3 x 3 λ_0) [14, 22].

c. Three-Dimensional T-Shaped Conducting Target [14, 22]

We next consider the monostatic RCS pattern of a T-shaped conducting target consisting of a 10 x 30 x 0.33 cm main plate and a 10 x 10 x 0.33 cm bisecting fin. The illumination is a 9.0-GHz plane wave at 0° elevation angle and TE polarization relative to the main plate. Thus, the main plate spans 9.0 λ_0. Note that look angle azimuths (as defined in Fig. 7) between 90° and 180° provide substantial corner reflector physics in addition to the edge diffraction, corner diffraction, and other effects found for an isolated flat plate.

For this target, the FD-TD model uses a uniform cell size of 0.3125 cm (λ_0/10.667), forming the main plate by 32 x 96 x 1 cells and the bisecting fin by 32 x 32 x 1 cells. The radiation boundary is located only 8 cells from the target's maximum surface extensions, so that the overall lattice size is 48 x 112 x 48 cells, containing 1,548,288 unknown field components (212.6 cubic wavelengths). Starting with zero-field initial conditions, 661 time steps are used, equal to 31 cycles of the incident wave.

Fig. 7 compares the FD-TD predicted monostatic RCS values at 32 key look angles with measurements performed by SRI International. These look angles are selected to define the major peaks and nulls of the monostatic RCS pattern. The agreement is excellent: in amplitude, within 1 dB over a 40-dB dynamic range; and in azimuth, within 1° in locating the pattern's peaks and nulls.

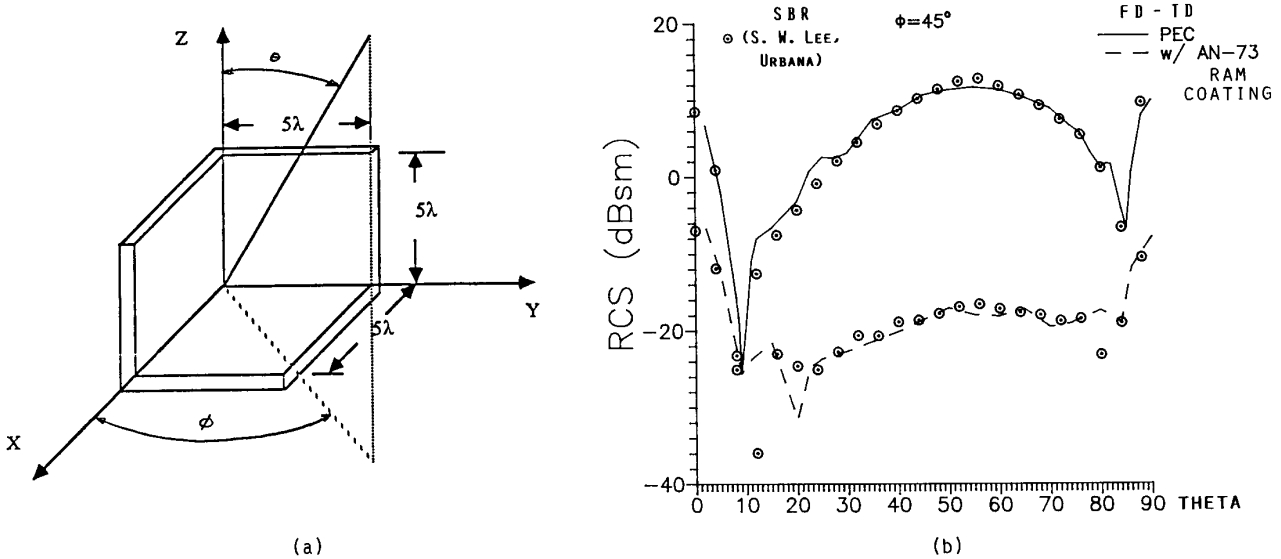

Fig. 8. Comparison of FD-TD and SBR results for the monostatic RCS vs. elevation angle of a trihedral corner reflector (both uncoated and with commercial RAM coating): (a) target geometry; (b) comparative RCS.

d. Trihedral Corner Reflector

We last consider the monostatic RCS pattern of a conducting trihedral corner reflector, both uncoated and with commercial radar absorbing material (RAM) coating. The reflector consists of three, thin, 15 x 15 cm flat plates mounted at mutual 90° angles, as shown in Fig. 8a. The illumination is a 10.0-GHz plane wave at 45° azimuth angle and θ-directed E field. Thus, the reflector spans 5 x 5 x 5 λ_o. For the coated case, the RAM is assumed to be Emerson & Cuming Type AN-73 (0.9525 cm thick, consisting of 3 distinct lossy layers of equal thickness).

For this target, the FD-TD model uses a uniform cell size of 0.25 cm (λ_o/12), spanning each plate by 60 x 60 cells. The lattice radiation boundary is located only 12 cells from the target, so that the overall lattice size is 84 x 84 x 84 cells, containing 3,556,224 unknown field components (343 cubic wavelengths). Starting with zero-field initial conditions, 720 time steps are used, equal to 30 cycles of the incident wave.

Fig. 8b compares the FD-TD computed monostatic RCS pattern in the θ plane (φ fixed at 45°) with predictions made by a shooting and bouncing ray (SBR) code developed by Prof. S. W. Lee of the University of Illinois at Urbana. Excellent agreement is seen for the uncoated target case. For the RAM-coated case, both codes predict substantial reduction of the RCS response. It is seen that the predicted RCS patterns for this case are in good qualitative agreement.

4. Potential for Modeling Ultra-Complex Targets

A graphic illustration of the potential of FD-TD for modeling structures comprised of ultra-complex electromagnetic wave absorbing media is provided by the whole-body dosimetry work reported by the University of Utah in [23]. Directly exploiting the ability of FD-TD to model media inhomogeneities down to the space-cell level, and fully utilizing the speed and memory capabilities of the Cray-2, highly realistic 3-D tissue models of the complete human body at a uniform space resolution in the order of 1 cm have been constructed for the first time. With capabilities of supercomputers expanding by at least one order of magnitude in the next decade, it is likely that FD-TD numerical modeling will occupy an important place in RCS technology in the 1990's and beyond.

Acknowledgement

This work was supported in part by ONR Contract N00014-88-K-0475, General Dynamics PO 4059045, and Cray Research, Inc. The help of Mr. Thomas Moore is gratefully acknowledged.

References

[1] K. Yee, "Numerical solution of initial boundary value problems involving Maxwell's equations in isotropic media," IEEE Trans. Antennas Propagat., AP-14, 302-307, May 1966.

[2] A. Taflove and M. Brodwin, "Numerical solution of steady-state electromagnetic scattering problems using the time-dependent Maxwell's equations," IEEE Trans. Microwave Theory Tech., MTT-23, 623-630, August 1975.

[3] G. Kriegsmann, "Exploiting the limiting amplitude principle to numerically solve scattering problems," Wave Motion 4, 371-380, 1982.

[4] A. Taflove and M. Brodwin, "Computation of the electromagnetic fields and induced temperatures within a model of the microwave irradiated human eye," IEEE Trans. Microwave Theory Tech., MTT-23, 888-896, Nov. 1975.

[5] A. Taflove and K. Umashankar, "Evaluation of time-domain electromagnetic coupling techniques," Final Report RADC-TR-80-251, Rome Air Dev. Ctr., Griffiss AFB, NY, April 1980.

[6] A. Taflove, "Application of the finite-difference time-domain method to sinusoidal steady-state electromagnetic penetration problems," IEEE Trans. Electromagn. Compat., EMC-22, 191-202, Aug. 1980.

[7] A. Taflove and K. Umashankar, "A hybrid moment method / finite-difference time-domain approach to electromagnetic coupling and aperture penetration into complex geometries," IEEE Trans. Antennas Propagat., AP-30, 617-627, July 1982.

[8] R. Holland, "Threde: a free field EMP coupling and scattering code," IEEE Trans. Nuclear Sci., NS-24, 2416-2421, Dec. 1977.

[9] K. Kunz and K. Lee, "A three-dimensional finite-difference solution of the external response of an aircraft to a complex transient EM environment: Part I," IEEE Trans. Electromagn. Compat., EMC-20, 328-333, May 1978.

[10] D. Meriwether, R. Fisher, and F. Smith, "On implementing a numerical Huygen's source scheme in a finite-difference program to illuminate scattering bodies," IEEE Trans. Nuclear Sci., NS-27, 1819-1833, Dec. 1980.

[11] G. Mur, "Absorbing boundary conditions for the finite-difference approximation of the time-domain electromagnetic field equations," IEEE Trans. Electromagn. Compat., EMC-23, 377-382, Nov. 1981.

[12] K. Umashankar and A. Taflove, "A novel method to analyze electromagnetic scattering of complex objects," IEEE Trans. Electromagn. Compat., EMC-24, 397-405, Nov. 1982.

[13] A. Taflove and K. Umashankar, "Radar cross section of general three-dimensional scatterers," IEEE Trans. Electromagn. Compat., EMC-25, 433-440, Nov. 1983.

[14] A. Taflove, K. Umashankar, and T. Jurgens, "Validation of FD-TD modeling of the radar cross section of three-dimensional structures spanning up to nine wavelengths," IEEE Trans. Antennas Propagat., AP-33, 662-666, June 1985.

[15] B. Engquist and A. Majda, "Absorbing boundary conditions for the numerical simulation of waves," Math. Comp. 31, 629-651, July 1977.

[16] G. Kriegsmann and C. Morawetz, "Solving the Helmholtz equation for exterior problems with variable index of refraction: I," SIAM J. Sci. Stat. Comput. 1, 371-385, Sept. 1980.

[17] A. Bayliss and E. Turkel, "Radiation boundary conditions for wave-like equations," Commun. Pure Appl. Math. 33, 707-725, 1980.

[18] L. Trefethen and L. Halpern, "Well-posedness of one-way wave equations and absorbing boundary conditions," Inst. Comput. Appl. Sci. and Eng. (ICASE), NASA Langley Res. Center, Hampton, VA, Report 85-30, June 1985.

[19] J. Blaschak and G. Kriegsmann, "A comparative study of absorbing boundary conditions," J. Comp. Physics 77, 109-139, July 1988.

[20] J. Blaschak, "Radiation boundary conditions: I. Absorbing boundary conditions for electromagnetic wave propagation," Ph.D. dissertation, Northwestern University, Evanston, IL, Aug. 1988.

[21] J. Fang and K. Mei, "A super-absorbing boundary algorithm for solving electromagnetic problems by time-domain finite-difference method," Proc. 1988 IEEE AP-S Symp., Syracuse, NY, June 1988, 472-475.

[22] A. Taflove, "Review of the formulation and applications of the FD-TD method for numerical modeling of EM wave interactions," Wave Motion 10, Dec. 1988.

[23] D. Sullivan, O. Gandhi, and A. Taflove, "Use of the finite-difference time-domain method in calculating EM absorption in man models," IEEE Trans. Biomed. Eng. 35, 179-186, March 1988.